ELSEVIER

Journal of Hazardous Materials 45 (1996) 27–44

JOURNAL OF HAZARDOUS MATERIALS

An analysis of the mechanisms of overpressure generation in vapour cloud explosions

R. Philip Cleaver, Clive G. Robinson*

British Gas plc, Research and Technology, Gas Research Centre, Ashby Road, Loughborough, Leicestershire LE11 3QU, UK

Received 20 August 1994; accepted 5 May 1995

Abstract

This paper describes an analysis of data obtained from explosion experiments carried out as part of the CEC (Commission of the European Communities) collaborative project MERGE (Modelling and Experimental Research into Gas Explosions). Previously established theoretical ideas are extended to obtain a simple relationship between the flame position and the overpressure as a function of time. The observed overpressure measurements and this relationship are then used to calculate the flame position as a function of time. The results of the analysis are shown to be consistent with the measurements made in the experiments. The technique is then used to identify the contribution to the overpressure from individual terms such as obstacle drag. It is concluded that the observed behaviour can be interpreted satisfactorily by this simple method and further that the approach itself could be embodied in a predictive technique.

Keywords: Vapour cloud explosions; Overpressure; Safety; Major hazards

1. Introduction

There is an increasing requirement to assess the safety of, and potential hazards posed by, both existing and proposed chemical and gas process plant. Necessarily, these safety assessments must consider the consequences of the accidental releases of liquids or gas. Although extremely rare, serious accidents can happen, e.g. [1,2]. The response to these accidents has been at several levels. In the UK there is now a requirement for Safety Reports and inspection by independent Health and Safety Executive inspectors of major sites. On the technical side, and in addition to in-house

* Corresponding author. Tel.: 01509 282445, Fax: 01509 283119.

Elsevier Science B.V.
SSDI 0304-3894(95)00063-1

work, companies and research organisations are encouraged by financial contributions by the CEC (Commission of the European Communities) to form collaborative projects to provide information from which hazards can be assessed more accurately.

One particular example of the latter is the project MERGE (Modelling and Experimental Research into Gas Explosions). This paper describes briefly the project MERGE and its aims, experimental data are taken from one component part of the project to develop established theoretical ideas and these are used to make predictions which are compared with the experimental data. The paper concludes with discussion of the findings of the analysis.

2. Project MERGE

The general objective of the MERGE project, described fully in [3], was to improve the understanding of gaseous explosions, and to use this to make more reliable predictions of the effects of such explosions in practice. To this end several experimental studies of gas explosions, including small-, medium- and large-scale experiments, were carried out. Also, various CFD (computational fluid dynamics) modelling techniques were used to simulate the experiments, the predictions compared and improvements made to the models, as proved necessary.

The British Gas experimental contribution consisted of a medium- and large-scale test program to study explosions in cube-shaped regions containing a regular pipework array. An example of the type of rig used is shown in Fig. 1(a). The experiments were conducted in an enclosure measuring $4.5 \times 4.5 \times 2.25$ m high for the medium-scale experiments and $9.0 \times 9.0 \times 4.5$ m high for the large-scale experiments. Placed within this region were six different types of obstacle arrays, details of the which are given in Table 1. Each obstacle array was formed from a number of circular cross-section tubes of the same diameter. These were arranged with a single spacing between pipes in each orthogonal direction. An element of this array is shown in Fig. 1(b). The fuels used were methane, a methane/propane mixture (3 parts methane to 1 part propane by volume), propane and ethylene. All these fuels were premixed with air in stoichiometric ratios. Some methane, methane/propane and propane experiments with oxygen enriched air were carried out at medium scale. Only the tests using methane, methane/propane and propane with air mixtures will be discussed in this paper.

All fuel/air mixtures were quiescent at the time of ignition. The ignition point was at ground level at the centre of the congested region and in the middle of the square produced by the nearest vertical pipes. Therefore, assuming the ground surface can be regarded as a plane of symmetry, the experiments approximately represented a central ignition of a cube-shaped congested region in free air. Prior to ignition of the fuel/air mixture, the polythene sheet covering the rig was cut by low-energy detonating chord. Instrumentation included pressure transducers and flame ionisation probes. The position of the instrumentation is shown in Fig. 2. Six pressure transducers were located at ground level along an orthogonal axis within the congested region. Other

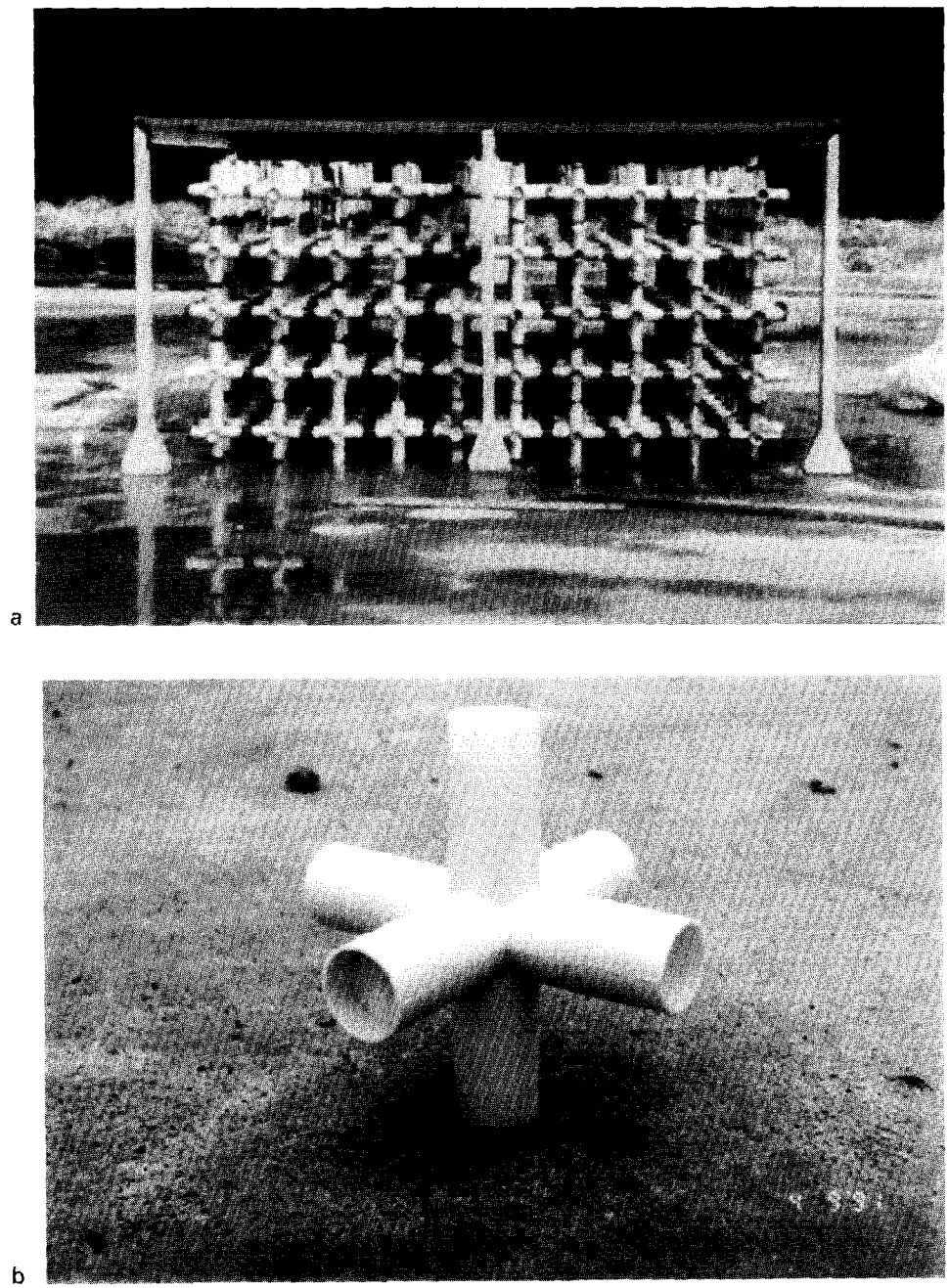

Fig. 1. One of the experimental rigs used for British Gas MERGE experiments showing (a) the complete rig and (b) an element of the obstacle array.

Table 1
Details of the congested regions used in the British Gas MERGE experiments

Grid type	Dimensions of congested region (m)	Pipe diameter (m)	Pipe spacing (m)
A	4.0 × 4.0 × 2.0	0.043	0.200
B	4.0 × 4.0 × 2.0[a]	0.041	0.133
C	4.0 × 4.0 × 2.0	0.086	0.400
D	4.3 × 4.3 × 2.1	0.082	0.267
E	8.0 × 8.0 × 4.0	0.168	0.800
C*	7.6 × 7.6 × 3.7	0.082	0.384

[a] For the propane test this was reduced to 3.5 × 3.5 × 1.7 due to the high overpressures obtained in the methane/propane test.

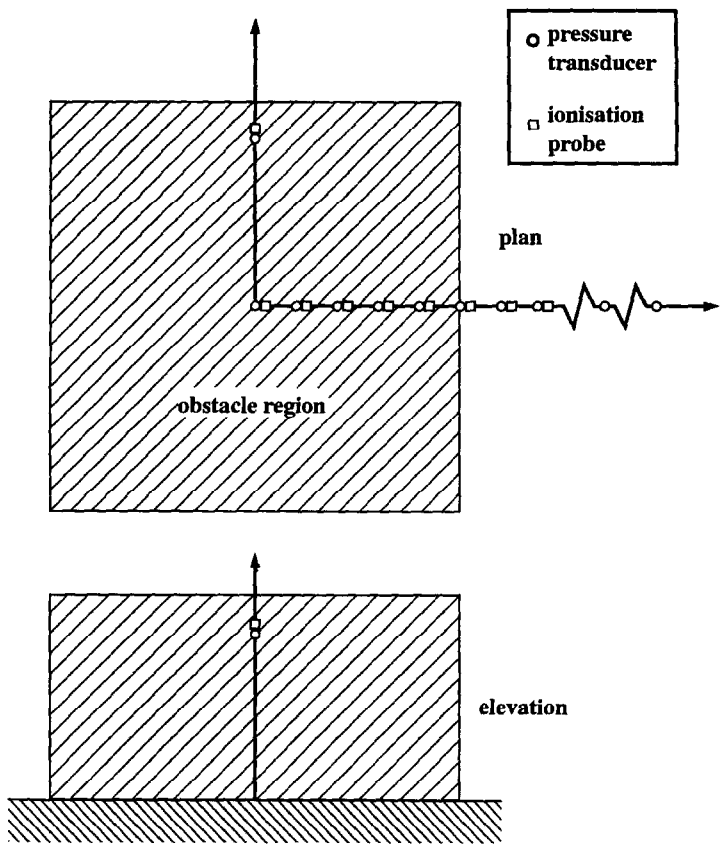

Fig. 2. Position of instrumentation in the British Gas MERGE experiments.

transducers were mounted along the other horizontal axis, the vertical axis, immediately outside the rig and in the far field. Flame ionisation probes were mounted alongside each of the pressure transducers inside and those immediately outside the congested region. High-speed cine (500 frames per second) and video records were also taken.

3. Simplified mathematical analysis of experiments

There are a number of techniques that can be used to analyse the relationship between flame propagation and the resulting overpressure. These range from, at the simplest level, acoustic models [4], incompressible models [5] and models based on the method of characteristics [6] to complex CFD models (see Annex 2 of [3]). In this paper we choose to use a simple approach based upon work described in [5], in which the flow was assumed to be incompressible and the flame was represented by a piston. This analysis has been extended to allow for the presence of the obstacles and some of the effects of compressibility have been included in a simple fashion. Also the method has been applied to experiments of a much larger scale and correspondingly higher flame speeds and overpressures than was the case in [5]. The derivation of the governing equations is given in Appendix A.

The result of the analysis is an algebraic expression for the non-dimensional pressure at the flame front, Eq. (A.10), in terms of the flame development and the geometrical and thermodynamic properties of the congested region and fuel/air mixture, respectively. In forming this relationship we have assumed

(a) complete combustion as the flame passes into the mixture ahead of it,

(b) uniform conditions behind the flame,

(c) instantaneously there is an incompressible flow field ahead of the flame,

(d) adiabatic compression of the fluid ahead of the flame,

(e) the total drag of one obstacle can be represented by the sum of its inertial and form drag,

(f) the total drag of the obstacles can be represented by the sum of the drag of each obstacle,

(g) the half-cube-shaped region can be mapped onto a hemisphere of equal volume.

In the following section this relationship between the flame and overpressure development is used to analyse the MERGE experiments described above.

4. Analysis of the British Gas MERGE experiments

Fig. 3 shows typical experimental results obtained from the flame ionisation probes and pressure transducers. Fig. 3(a) shows the flame at first progressing relatively slowly and eventually accelerating rapidly as it passes from the ignition point through the obstacle array. The associated large pressure rise, Fig. 3(b), is seen to coincide with this rapid acceleration phase, as expected.

To examine the validity of the theoretical approach, given in Appendix A, the information on flame position against time obtained from the ionisation probe data could be used to predict the overpressure as a function of time, and then these predictions could be compared with the experimentally measured overpressures. However there are several disadvantages to this approach, particularly the need to numerically differentiate the flame position against time data to determine the flame speed and again to determine the flame acceleration. The uncertainties involved in these operations are large, particularly for high flame speeds when the differences in

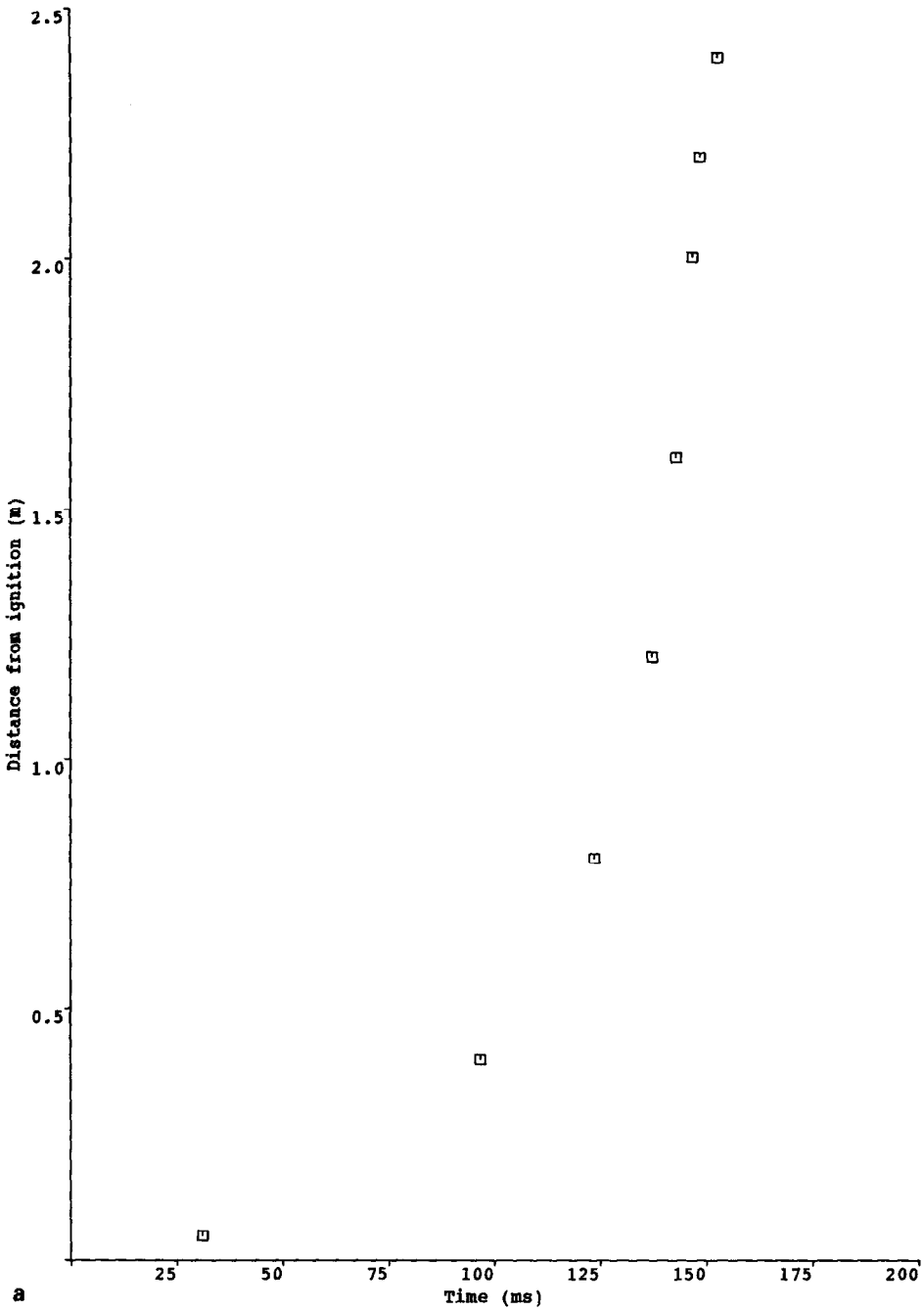

Fig. 3. Example results from (a) the flame ionisation probes and (b) a pressure transducer.

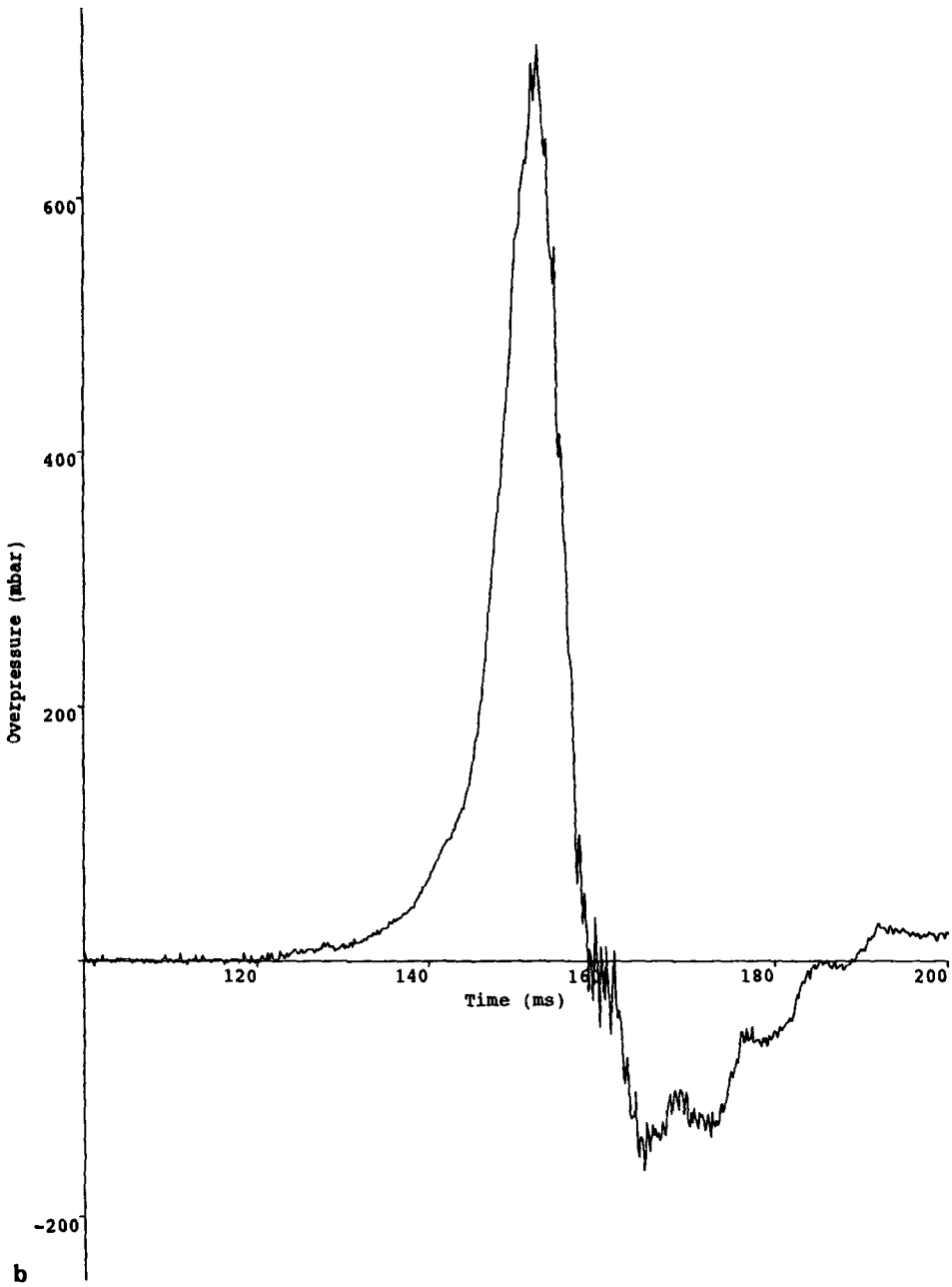

Fig. 3. Continued.

arrival times between adjacent ionisation probes is sometimes less than 1 ms. Also flame distortion effects at the higher flame speeds sometimes lead to an ionisation probe detecting the flame before the probe closer to the ignition point has detected it. Using these data would give rise to negative values of flame speeds, whereas in reality the rate of progress averaged over the whole flame front is positive.

Hence, an alternative approach has been taken, as suggested in [5] and [6], in which Eq. (A.10) has been integrated numerically using the pressure transducer measurements to obtain the flame position as a function of time. This procedure is preferable numerically and also physically, as there are many more measurements contained in the pressure transducer data than the ionisation probe data. In order to do this, the overpressure at the flame front is required and this has been inferred from the experimental measurements, which were taken at fixed points in space, as follows. It might be expected that, due to the geometry in question and the high speed of sound in the burnt products behind the flame, that the overpressure behind the flame would be uniform. Indeed this is confirmed by the typical experimental measurements shown in Fig. 4. In Fig. 4 the overpressure measurements from eight transducers have been used to produce a contour map of overpressure. Also shown in Fig. 4 is the flame position given by the ionisation probe data and that calculated from Eq. (A.10) and the pressure transducer data. It can be seen that at any instant the overpressure behind the flame front is approximately uniform, whilst there is a pressure gradient ahead of the flame. Therefore, pressure transducer data from behind the flame front can be used to represent the overpressure at the flame front itself.

In practice, it was found that due to the relatively small pressure rise in the early part of the experiments, data from a single pressure transducer could be used. Further, the results were not sensitive to which pressure transducer data was used, provided that it was within the congested region. However, the integration had to be started at a time after the pressure transducers begin to record more signal than noise. If information was used from earlier times in the experiment, the noise could give rise to spurious results. When this start time had been chosen, initial conditions for the dependent variables of the integration, i.e. flame radius and flame speed, could be calculated from the appropriate ionisation probe data.

The results of this analysis are shown in Fig. 5 for all the British Gas MERGE experiments. Also shown, as symbols, are the corresponding flame positions derived from the ionisation probe data.

5. Discussion

From Fig. 5 it can be seen that in general the results of the analysis and the ionisation probe data agree reasonably well showing the overall validity of the approach. Fig. 5 shows comparisons from the medium (grid types A, B, C and D) and large-scale (grid types E and C*) experiments. Table 1 gives details of the congested regions used in these experiments.

The first set of results for the A rig show good agreement for all three fuels with the predicted flame positions (lines) being almost exactly the same as the measured flame positions (symbols).

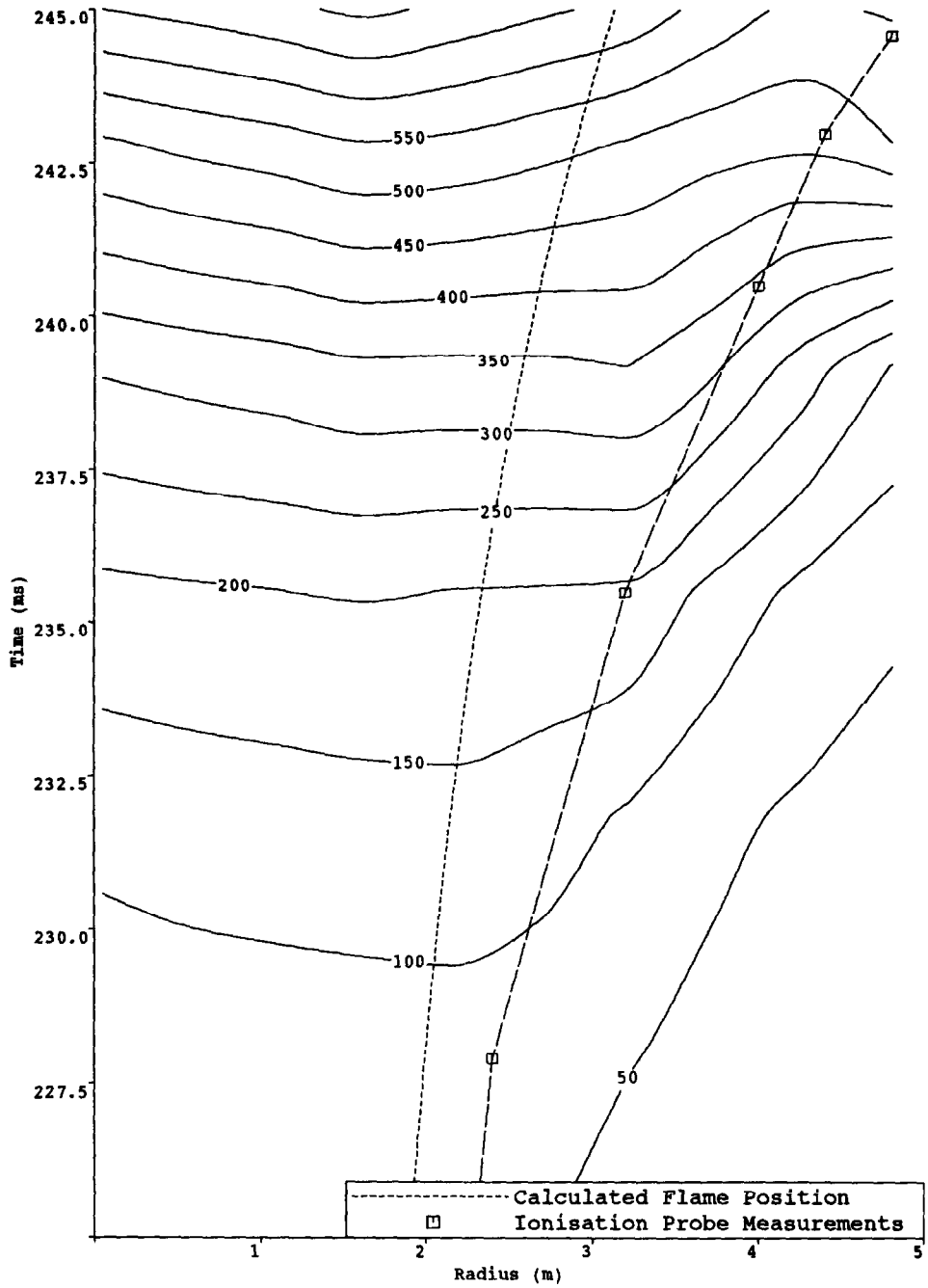

Fig. 4. Contour map of overpressure (mbar) and flame position as a function of time showing uniform pressure behind the flame front.

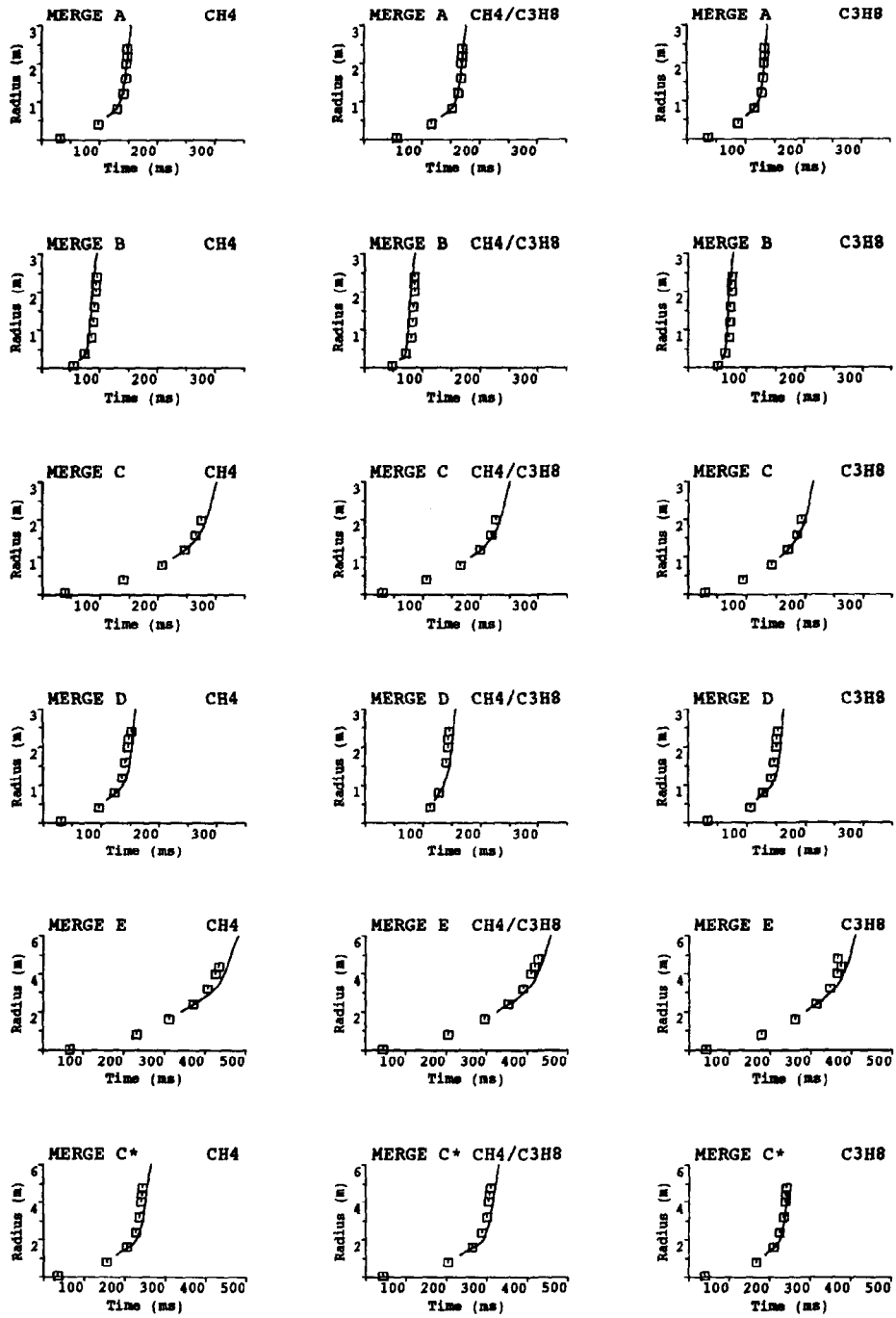

Fig. 5. Comparisons between ionisation probe data (□) and flame radius as a function of time derived from pressure transducer data (–).

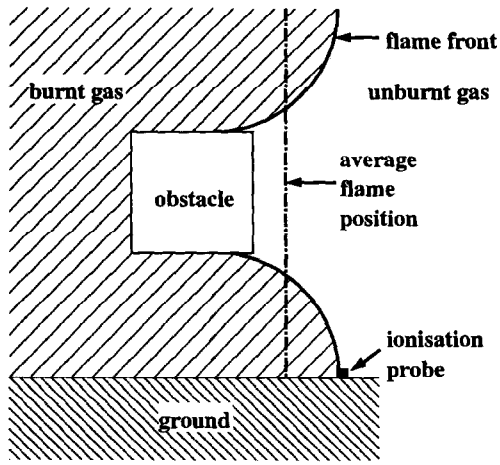

Fig. 6. Flame distortion around an obstacle.

The comparisons for the B experiments appear to show reasonable agreement, but it can be seen that this is the only set of comparisons in which the predicted flame position is in front of the measured position. In fact, it is expected that the measured flame position should be slightly in front of the predicted position. This is because the measurements indicate the leading edge of the flame and if the flame front is distorted, which it will be as it flows around the obstacles, this will be ahead of the average position predicted by the theoretical approach. This situation is shown in Fig. 6. Also closer inspection of the predicted flame position shows the flame beginning to decelerate at a radius of approximately 2 m for all fuels whilst the measurements indicate a continued acceleration. Again this disagreement is not found in any other comparisons. These experiments produced the highest overpressures and flame accelerations of all the tests, the propane test giving overpressures and flame speeds of approximately 4 bar and 300 m/s, respectively. This is discussed further below.

The third set of comparisons for the C experiments show good agreement. However, due to the fact that there were fewer pressure transducers in these experiments and overpressures were lower, which meant that the integration had to be started at a later time, there were fewer points to compare.

The comparisons for the D experiments also show good agreement although the measured flame positions are consistently in front of the predicted ones. The overpressures and flame speeds were similar to those produced in the A experiments and it is not clear why the agreement is better for the A experiments. One possible explanation is that the D experiments used fewer obstacles than the A experiments but of a larger size and this may have caused larger flame distortion resulting in the leading edge of the flame being further in front of the mean position than in the A experiments.

The comparisons for the E experiments show reasonable agreement. An inconsistency in the flame position obtained from the ionisation probe data can be seen for the

final probe in the propane experiment which detected the flame before the penultimate one.

Finally, comparisons for the C* experiments show good agreement. Consistently the flame position was predicted to be behind the leading edge of the flame given by the ionisation probe data.

From these comparisons it can be concluded that the theoretical approach is valid at all but the highest overpressures and flame speeds, which were observed in the B set of experiments. This lack of agreement between the predictions and the experimental measurements is due to the assumptions made within the model, notably the instantaneous incompressible flow field ahead of the flame, becoming invalid at the overpressures and flame speeds observed in the B experiments. It would appear from the comparisons that the model is reasonably valid up to flame speeds of approximately 250 m/s.

The calculated flame position as a function of time can be used as input to Eq. (A.10) to generate the corresponding overpressure. This is shown in Fig. 7, for the example of grid type D with methane as the fuel. Here the calculated non-dimensional overpressure, $f(P)$, defined as

$$f(P) = \left(\frac{p(R_f)}{p(\infty)}\right)^{(\gamma-1)/\gamma} - 1$$

is compared with the value deduced from the measurements. The two curves agree, as should be the case, as nothing more than numerical integration and then differentiation of a function has been carried out. (There is some smoothing out of some of the high-frequency fluctuations due to the numerical method used.) However this result suggests that if it were possible to predict the flame position as a function of time, for example by using a correlation, then this approach could be used to predict the overpressure. This technique also provides a method to determine the contribution to the overpressure from individual terms. This is also seen in Fig. 7, in which the terms representing the integrated effects of the fluid advection and acceleration and the drag of the obstacles ahead of the flame are shown. The individual terms are defined as

$$\text{fluid advection and acceleration} = \frac{(\gamma-1)}{a^2}(A - C),$$

$$\text{obstacle drag} = \frac{(\gamma-1)}{a^2}(B + D).$$

(The expressions for A, B, C, and D are given in Eq. (A.10) of Appendix A.) It can be seen that the drag due to the obstacles contributes much less to the total overpressure than the fluid advection and acceleration. These calculations have been carried out with a value of form drag, C_d, of 1.0. However, the analysis given in [7] suggests that in steady unidirectional flow the value of C_d should be increased by a factor of approximately 3 for grid type D. If this value is used for the transient situation then the contribution of the obstacle drag is approximately doubled, although it is still smaller than the contribution assigned to the fluid advection and acceleration. (It was found that the effects of changing C_d on the results shown in Fig. 5 were minimal.) The

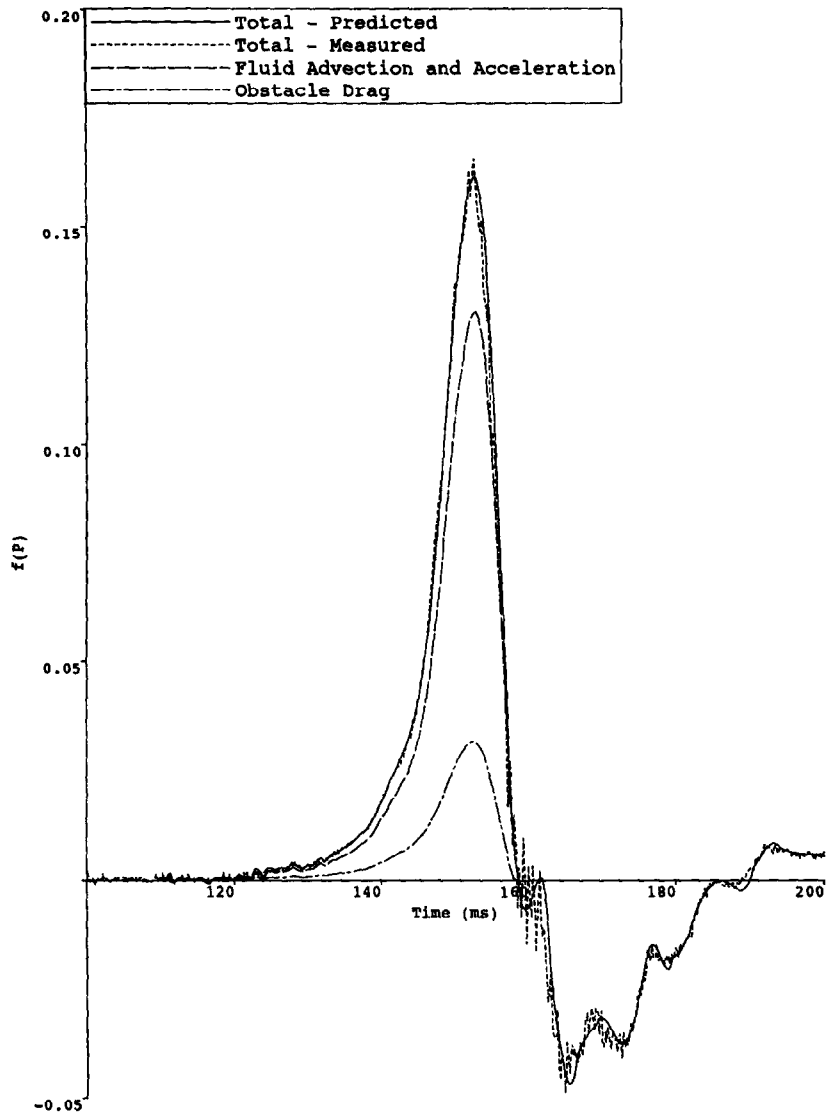

Fig. 7. Contributions of individual terms to the overpressure. (Grid type D, methane fuel.)

value of the relative contribution of the obstacle drag for experiments with lower volume blockages was found to be smaller. It can also be seen from Fig. 7 that the drag of the obstacles increases initially as the flame accelerates and then decreases, due to a combination of the flame deceleration and the presence of fewer obstacles between the flame front and the edge of the congested region. It finally becomes zero when the flame leaves the congested region at a time of 160 ms. The large deceleration of the flame is seen to be responsible for the negative overpressure pulse after the main positive pulse.

6. Conclusions

At a bulk level most of the behaviour of the medium- and large-scale MERGE vapour cloud explosion experiments, in terms of the flame propagation and corresponding overpressure development, can be explained by the simple theoretical approach taken in this paper. The approach is valid at flame speeds less than approximately 250 m/s.

The obstacles within the explosion do have a very large effect on the flame acceleration, through the generation of shear and turbulence in the flow ahead of the flame, which in turn generates overpressure. However, their contribution to the overpressure in terms of drag is less important than the advection and acceleration of the fluid itself at the levels of blockage studied (up to 20% volume blockage).

Acknowledgements

This paper is published by permission of British Gas plc.

This work has been performed as part of project EMERGE (Extended Modelling and Experimental Research into Gas Explosions) which is financially supported by the Commission of the European Communities, Directorate XII: Science, Research and Development in the field of Research and Technological Development under the STEP programme: Science and Technology for Environmental Protection.

The authors would like to thank both referees for their helpful comments.

Appendix A: A relationship between flame propagation and pressure

A.1. Derivation of equation for pressure

Fig. 8 shows a schematic diagram of the model for the propagation of a flame through an idealised geometrical arrangement of obstacles. A spherically symmetric piston at R_f, which represents the flame, moves through a region of obstacles which extends to R_c. Conditions in front of the flame are adiabatic. Outside R_c there are no obstacles and the conditions a long way from the congested region are ambient.

The equations to be solved are the conservation of mass and momentum. In spherical coordinates for symmetric flows these can be written as

$$\frac{\partial \rho}{\partial t} + \frac{1}{r^2}\frac{\partial \rho u r^2}{\partial r} = 0, \tag{A.1}$$

$$\frac{\partial u}{\partial t} + \frac{u \partial u}{\partial r} = \frac{-1}{\rho}\frac{\partial p}{\partial r} - f, \tag{A.2}$$

where f is the force per unit mass exerted by the fluid on the obstacles. For $r \leqslant R_c$ this can be expressed as

$$f = k_1 \frac{\partial u}{\partial t} + k_2 \tfrac{1}{2} u^2, \tag{A.3}$$

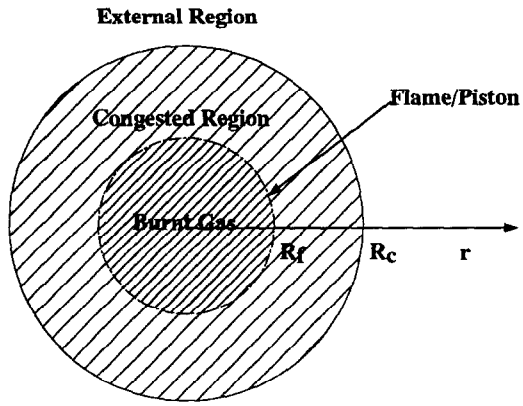

Fig. 8. Schematic diagram of the simple model.

where the first term represents the inertial drag and the second term the form drag of the obstacles. The constants k_1 and k_2 depend on the obstacle geometry and will be discussed in the next section. For $r > R_c$

$$f = 0$$

as there are no obstacles.

For $r \leqslant R_c$ the momentum equation can then be written as

$$(1 + k_1)\frac{\partial u}{\partial t} + k_2 \tfrac{1}{2}u^2 + \frac{\partial \frac{1}{2}u^2}{\partial r} = \frac{-1}{\rho}\frac{\partial p}{\partial r} \tag{A.4}$$

and for $r > R_c$

$$\frac{\partial u}{\partial t} + \frac{\partial \frac{1}{2}u^2}{\partial r} = \frac{-1}{\rho}\frac{\partial p}{\partial r}. \tag{A.5}$$

To include compressibility in a simple fashion ρ in Eqs. (A.4) and (A.5) has been expressed in terms of pressure, assuming an adiabatic compression. Thus

$$\frac{1}{\rho}\frac{\partial p}{\partial r} = \frac{p_0^{1/\gamma}}{\rho_0}\frac{\gamma}{(\gamma - 1)}\frac{\partial p^{(\gamma-1)/\gamma}}{\partial r}, \tag{A.6}$$

where γ is the ratio of specific heats of the fluid and ρ_0 and p_0 are a reference density and pressure, respectively. Substituting equation (A.6) into the sum of Eqs. (A.4) and (A.5) and integrating the resulting equation from R_f to the outer boundary at infinity gives

$$k_1 \int_{R_f}^{R_c} \frac{\partial u}{\partial t}\,dr + \int_{R_f}^{\infty} \frac{\partial u}{\partial t}\,dr + \int_{R_f}^{\infty} \frac{\partial \frac{1}{2}u^2}{\partial r}\,dr + k_2 \int_{R_f}^{R_c} \tfrac{1}{2}u^2\,dr$$
$$= \frac{-p_0^{1/\gamma}}{\rho_0}\frac{\gamma}{(\gamma - 1)}\int_{R_f}^{\infty} \frac{\partial p^{(\gamma-1)/\gamma}}{\partial r}\,dr. \tag{A.7}$$

In this equation the density of the air and the fuel/air mixture ahead of the flame have both been put equal to ρ as the difference for most fuels of interest within the flammable limits is small.

To evaluate the first, second and fourth integrals a velocity field must be specified. This has been done by treating the equation of conservation of mass as incompressible. Integrating Eq. (A.1) using this assumption gives

$$u(r) = u(R_f)\frac{R_f^2}{r^2}, \tag{A.8}$$

where $u(R_f)$ is the value of the velocity as the flame front is approached from the unburnt gas. This is a simplification which will become less valid for higher flame speeds.

Substituting Eq. (A.8) into (A.7) and integrating gives

$$\frac{p(R_f)}{p(\infty)} = \left(\frac{\gamma-1}{a^2}\left(\left(2u(R_f)\frac{dR_f}{dt} + R_f\frac{du}{dt}(R_f)\right)\left(1 + k_1\left(1 - \frac{R_f}{R_c}\right)\right)\right.\right.$$
$$\left.\left. - \frac{1}{2}u^2(R_f)\left(1 - k_2\frac{R_f}{3}\left(1 - \left(\frac{R_f}{R_c}\right)^3\right)\right) + 1\right)\right)^{\gamma/(\gamma-1)} \tag{A.9}$$

where the reference pressure p_0, and density ρ_0 have been set to $p(\infty)$ and $\rho(\infty)$, respectively, and a, the speed of sound in the ambient fluid, is given by

$$a = \sqrt{\frac{\gamma p(\infty)}{\rho(\infty)}}.$$

We now write

$$u(R_f) = S_f - S_u,$$

$$u(R_f) = S_f\frac{(E-1)}{E},$$

where S_u is the burning velocity, S_f is the flame speed and E is the expansion ratio of the fuel. The use of this single value of the expansion ratio infers that conditions behind the flame are uniform and the validity of this assumption is discussed in Section 4 of this paper. Using this relationship and noting that

$$\frac{dR_f}{dt} = S_f,$$

we obtain

$$\frac{p(R_f)}{p(\infty)} = \left(\frac{\gamma-1}{a_2}(A + B - C + D) + 1\right)^{\gamma/(\gamma-1)}, \tag{A.10}$$

where

$$A = \frac{(E-1)}{E}\left(2S_f^2 + R_f\frac{dS_f}{dt}\right),$$

$$B = k_1\left(1 - \frac{R_f}{R_c}\right)A,$$

$$C = \frac{1}{2}\left(S_f\frac{(E-1)}{E}\right)^2,$$

$$D = k_2\frac{R_f}{3}\left(1 - \left(\frac{R_f}{R_c}\right)^3\right)C.$$

This equation can be used to relate the value of the overpressure at the flame front to the flame position as a function of time. It is this relationship that is used in the analysis described in Section 4 of this paper.

A.2. Interpretation of the obstacle force term

An interpretation of the term k_1 can be obtained by considering the flow around single isolated obstacles as follows. The inertial drag part of the force on the obstacle can be written as, [8],

$$F = C_m V_o \rho \frac{\partial u}{\partial t},$$

where C_m is a constant, V_o is the volume of the obstacle and F is the force on the body. The constant C_m is equal to 1.5 for spherical bodies and 2.0 for cylindrical bodies. Integrating the inertial part of f over a volume V and multiplying by the density ρ we obtain

$$k_1 V \rho \frac{\partial u}{\partial t} = C_m V_o \rho \frac{\partial u}{\partial t},$$

which gives

$$k_1 = C_m V_b,$$

where V_b is the volume blockage of the obstacles. If we assume that the obstacles do not interact, which will be true in the limit of small V_b, we can therefore use this expression for arrays of obstacles.

The force due to the form drag can be written as, [8],

$$F = C_d \tfrac{1}{2}\rho A_o u^2$$

where C_d is the drag coefficient and A_o is the area of the object normal to the flow. In general this drag coefficient will be a function of the Reynolds number of the flow and the shape and orientation of the object. Integrating the form drag part of f over

a volume V and multiplying by the density we obtain

$$k_2 = C_d \frac{A_o}{V}.$$

If we assume that for an array of obstacles there is no interaction, which will be true in the limit of small $A_o d/V$, where d is the obstacle diameter, we can then write

$$k_2 = C_d \frac{A_t}{V},$$

where A_t is the total area of the obstacles normal to the flow within the volume V of the congested region. If interaction does occur then a modified value of C_d should be used to take this into account.

In the analysis of the experiments the value of A_t that was used was obtained assuming that the flow was perpendicular to one of the obstacle array coordinate directions. As the flow in the British Gas MERGE experiments is radially outwards from the ignition point, the flow is not in this direction for all of the obstacles. However, the variation of the projected area with flow direction is small and has been neglected in the analysis.

The constants C_m and C_d have been taken as 2.0 and 1.0, respectively, for all experiments.

References

[1] R.J. Parker (chrmn), The Flixborough Disaster. Report of the Court of Inquiry, HMSO, London 1975.
[2] J. Sambeth, Chem. Eng., May (1983).
[3] W.P.M. Merx, Modelling and experimental research into gas explosions, Overall Final Report of the MERGE project, CEC contract, STEP-CT-0111 (SSMA).
[4] G.I. Taylor, Proc. Roy. Soc., A186 (1946) 273–292.
[5] B. Deshaies and J.C. Leyer, Combust. Flame, 40 (1981) 141.
[6] R.A. Strehlow, L.D. Savage and G.M. Vance, Combust. Sci. Technol., 6 (1973) 307.
[7] S.F. Hoerner, Fluid Dynamic Drag, S.F. Hoerner, Midland Park, NJ, 1965.
[8] G.K. Batchelor, An Introduction to Fluid Dynamics, Cambridge Univ. Press, Cambridge, 1991.